Food Innovation and Advances

ARTICLE

Open Access

https://doi.org/10.48130/FIA-2023-0024

Food Innovation and Advances **2023**, 2(3):225–232

Photooxidation stability of phytosterols with different relative spatial positions in different particles

Jingjian Liu[1], Dan Wang[1], Ping Shao[1,2] and Simin Feng[1,2*]

[1] *Department of Food Science and Engineering, Zhejiang University of Technology, Hangzhou 310014, Zhejiang, China*

[2] *Key Laboratory of Food Macromolecular Resources Processing Technology Research (Zhejiang University of Technology), China National Light Industry, Hangzhou 310014, China*

* Corresponding author, E-mail: fengsimin@zjut.edu.cn

Abstract

The aim of this study was to investigate the effects of relative spatial position of stigmasterol on its photooxidation stability in different particles. Phytosterol oxidation products (POPs) from phytosterol oxidation were successfully isolated and studied using solid phase extraction (SPE) technology in conjunction with GC-MS. The photooxidation stability of stigmasterol in four particles was as follows: zein stabilized particles (ZPs) ≈ zein-pectin stabilized particles (ZPPs) > soy protein isolate (SPI)-pectin stabilized particles (SPPs) > SPI stabilized particles (SPs). 7β-Hydroxy and 5β, 6β-epoxy was the main POPs in the first and second oxidation stages, respectively, which reached 8,945 ± 43 μg/g and 6,010 ± 289 μg/g after 240 min UV light exposure treatment in SPs. When stigmasterol was hydrophobically adsorbed on the surface of SPs, the network gel generated by pectin outside SPPs prevented photooxidation of stigmasterol. When stigmasterol was encapsulated in the interior of ZPs, the blocking effect of pectin in ZPPs became insignificant. The study provided a feasible development direction for the storage and quality control of phytosterols as dietary supplements.

Citation: Liu J, Wang D, Shao P, Feng S. 2023. Photooxidation stability of phytosterols with different relative spatial positions in different particles. *Food Innovation and Advances* 2(3):225–232 https://doi.org/10.48130/FIA-2023-0024

Introduction

Phytosterols (PSs) are a class of natural compounds with molecular structures similar to cholesterol[1]. PSs are abundant in nature, particularly in oil seeds like rapeseed, soybean, and corn[2]. Since the 1950s, PSs have been recognized to have a number of biological features, including lowering total cholesterol and low-density lipoprotein cholesterol levels[3,4]. Additionally, recent studies have demonstrated that PSs are crucial for avoiding colitis[1] and non-alcoholic fatty liver disease[5]. Currently, hydrophilic phytosterol derivatives are more widely used in the food industry than free phytosterols[6]. PSs are added to many foods as dietary supplements, such as yogurt, margarine and corn oil. The development of functional foods rich in PSs will have broad application prospects. Similar to cholesterol, PSs is readily oxidized and converted to hydroxyl, epoxy, and keto derivatives, which are known as the products of phytosterol oxidation (POPs)[7]. Many studies have shown that POPs are related to various health problems, which causes serious safety concerns about functional foods rich in PSs. For example, elevated POPs levels can cause coronary artery disease and atherosclerotic cardiovascular disease[8]. Moreover, POPs express varying levels of cytotoxicity[7]. Although the mechanism and regulation of dietary PSs' thermal oxidation have been extensively investigated, information about their photooxidation of PSs remains unclear and limited. PSs' photooxidation is initiated by singlet oxygen ($^1O_2$), which is converted from ozone under natural light or ultraviolet light and is 1500 times more reactive than ozone[9].

According to several studies, nano-encapsulation can significantly increase the functional components' oxidation stability. Zein, a hydrophobic protein, can self-assemble into nanoparticles with various microstructures[10]. It exhibits excellent thermal resistance, oxygen barrier, antioxidation properties, and low hygroscopicity[11]. The flexibility and oxygen barrier qualities of zein have been improved using a variety of hybrid techniques. Wang et al.[12] loaded curcumin into zein nanofibril films of konjac glucomannan (KGM) by means of the electrospinning method. In comparison to pure KGM and zein, the oxidation stability of the KGM-zein nanofibril films was improved. Zhang et al.[13] prepared chitosan/zein nanoparticles, which showed improved barrier properties of water vapour, oxygen and carbon dioxide as compared to neat chitosan. However, because of the small size and high specific surface area of the nanoparticles, some studies have shown that functional components are prone to oxidation following nano encapsulation. For example, curcumin was complexed with soy protein isolate (SPI) at pH 3.0 and 7.0[14]. At both pH levels, the complexes that were created at the nanoscale greatly sped up the emulsion's lipid oxidation. The specific mechanism of nano-encapsulation in improving or impairing the oxidation stability of bioactive compounds is still unclear. We hypothesized that the oxidation stability of bioactive compounds is related to the chemical properties of wall materials and their spatial position in particles.

Phytosterol esters were demonstrated to be adsorbed on the surface of SPI particles (SPs) by hydrophobic contact in our earlier work[15]. Meanwhile, PSs were encapsulated in the interior of zein particles (ZPs) during the self-assembly process[16].

We supposed that the network gel formed by pectin outside the particles could prevent stigmasterol from being directly exposed to UV light in SPI-pectin stabilized particles (SPPs). However, the blocking effect on stigmasterol in zein-pectin stabilized particles (ZPPs) was not significant, because stigmasterol was encapsulated in the interior of ZPs.

We chose zein, SPI, and pectin as wall materials for stigmasterol particles in this investigation. The aim was to determine the effects of the relative spatial position of stigmasterol on the photooxidation stability of stigmasterol particles. We looked into how different wall materials affected microstructure, photooxidation stability, average particle size, zeta-potential, and particle contact angle. The results of this study should provide guidance for the control of dietary quality of dietary supplements containing phytosterols in the industry.

Materials and methods

Materials

Zein was bought from the company Sinopharm Chemical Reagent Co., Ltd. (China). Stigmasterol (95% purity) was purchased from Xian Healthful Biotechnology Co., Ltd. (Xi'an China). Soybean protein isolate (SPI) (purity > 90%) was purchased from Shandong Sinoglory Health Food Co., Ltd. (China). Pectin was bought from Sigma Chemical Co. in St. Louis, Missouri, USA. All substances used in this research was of analytical grade.

Fabrication of stigmasterol particles

ZPs and ZPPs were made according to the instructions in our prior work[17], while the preparation of SPs and SPPs referred to another study[18]. Briefly, the solution of stigmasterol (2 mg/mL) was made by taking up stigmasterol in anhydrous ethanol and then placing it in a 45 °C water bath for ease of dispersion. With agitation, deionized water (50 mL) was added to contain approximately 50 mg of SPI and 0~5 mg of pectin (pectin/SPI mass ratios of 0:10 and 1:10). Stigmasterol solution was added incrementally to SPI-pectin solution at a flow rate of 2 mL/min while being sheared at a high speed of 10,000 rpm. Under optimum fabrication circumstances, the coarse emulsion was cured for 3 min. A rotary vacuum evaporator was then used to remove the organic solvent at 45 °C until the volume was no longer changing.

Particle effectiveness in encapsulation (EE) and loading amount (LA) determination

According to the approach by Feng et al.[17], the encapsulation effectiveness (EE) and loading amount (LA) of the particles were determined. Stigmasterol in particles was extracted with a certain amount of n-hexane under oscillating conditions. The n-hexane layer was subsequently added to 15 mL tubes of a centrifuge and dried using a centrifuge concentrator under vacuum after layering. After that, the dried samples were redissolved in 100% ethanol and measured using the previously mentioned methods[16]. The following formulas were used to calculate the EE% and LA (g/100 g):

$$EE\% = \frac{Total\ stigmasterol\ amount - Unencapsulated\ stigmasterol}{Total\ stigmasterol\ amount} \times 100\% \quad (1)$$

$$LA = \frac{Total\ stigmasterol\ amount - Unencapsulated\ stigmasterol}{Total\ zein/pectin\ amount} \times 100 \quad (2)$$

Particulate microstructure

Particle microstructure was assessed by the method outlined by Feng et al[16]. Briefly, a transmitted light scanning electron microscopy (Model Nano nova 450, FEI Instruments Co., USA) was used to evaluate the appearance of particles (ZPs, ZPPs, SPs, and SPPs). For 48 h, the samples were freeze-dried in a vacuum. Conductive double-tape was attached to the freeze-dried particles, which was then placed on a SEM tray. The powder on the tape was spread out, and the loose pieces were blown away, using a blow-rubber ball. The tape was subsequently examined using SEM.

Particle size and zeta potential analysis

The properties of particles in dispersions were explored using dynamic light scattering (DLS) technique. The average particle diameter was determined using a particle dimension analyzer. The same device was used to calculate the zeta-potential in PALS Zeta Potential Measurement mode.

UV light exposure treatment

The newly prepared particles (ZPs, ZPPs, SPs and SPPs) were placed in culture dishes and exposed to UV light (15 W) at 25 °C. At 30, 60, 90, 120, 150, 180 and 240 min, approximately 25 mL of samples were collected each time. In order measure the amount of residual stigmasterol and the consequent POPs, samples were maintained at −20 °C until analysis.

Quantification of stigmasterol and POPs

Quantification of stigmasterol and POPs was performed using the method described in a previous study[19], with slight modifications. Briefly, 10 mL of diethyl ether and 10 mL of water were added to the samples to dissolve the remaining stigmasterol and resulting POPs. The procedure was repeated three times, and the top phase was collected and dried over nitrogen. The dried samples were then redissolved in a 1 mL n-hexane/diethyl ether (V:V = 9:1) solution.

After activating the SIOH-SPE cartridge with 5 mL of n-hexane, 1 mL of oxidized sample was loaded. Five mL of n-hexane/diethyl ether (V:V = 1:1) was used to elute the unoxidized stigmasterol. POPs were then eluted using 5 mL of acetone. As internal standards, 10 L of 5-cholestane (50 g/mL in acetone) and 10 L of 19-hydroxycholesterol (50 g/mL in acetone) were added. The extracts were then nitrogen-dried before being redissolved in 100 L of pyridine. The reaction mixture was then silylated overnight at room temperature with BSTFA/TMCS (100 L), followed by reagent evaporation, and the residue was redissolved in 200 L n-hexane for GC-MS analysis.

In an Agilent 7890B GC (Agilent, Santa Clara, CA, USA) fitted with a Gerstel MPS autosampler (Gerstel, Germany) and connected to an Agilent 5977 MSD detector (Agilent, San Clara, CA, USA), a TG-5MS (30 m × 0.25 mm × 0.25 μm, Agilent Technologies, USA) separated individual PSs and POPs. PSs and POPs were tracked in SIM mode. The following were the GC conditions: Helium (99.999%) streamed as the carrier gas at an average velocity of 1.0 mL/min. The oven's temperature was first set at 90 °C for 1 min, then increased gradually to 270 °C at a rate of 30 °C/min, and then increased to 300 °C at a rate of 3 °C/min for 10 min. The following were the MS symptoms: 280 °C for the interface, 250 °C for the ion source, and 70 eV for electron impact (EI) to cause ionization.

The contents of stigmasterol and POPs were calculated as follows:

$$m_c = \frac{A_c}{A_{is}} m_{is} RRF_c$$

where m_c and m_{is} are the masses of the target and the internal standard, respectively. A_c and A_{is} are the peak areas of the target and the internal standard, respectively. RRF_c is the correction factor of the target relative to the internal standard which is approximate.

Three-Phase Contact Angle

Three-Phase Contact Angle was determined using the method in a previous study[20], with slight modifications. After the lyophilized particles (0.1 g) were pressed into cylindrical tablets (10 mm × 2 mm), the three-phase angle of contact was measured using an optical contact angle meter (OCA 20, Data Physics Instruments GmbH, Germany). Briefly, 10 L of particles were softly pushed out of the syringe and instantly stuck to the tablet's surface after the tablet had been submerged in pure corn oil. A camera was used to capture the shape of the droplet, and the Laplace-Young equation was used to determine that shape.

Statistical analysis

Every study were conducted in triplicate, and the results were reported as the mean standard deviation. The Statistical Program for Social Science application (SPSS 24.0, Chicago, IL, USA) was used for all statistical analysis. The analysis of variance (ANOVA) significance level was established at 0.05.

Results and discussion

Microstructure of particles

The EE% and LA (g/100 g) of ZPs were 90.11 ± 2.05% and 94.86 ± 1.03 g/100 g, respectively. Compared with ZPs, the addition of pectin slightly decreased the EE% and LA (g/100 g) slightly in ZPPs, possibly due to the stronger electrostatic interaction provided by pectin. However, the EE% and LA (g/100 g) of all four types of particles (ZPs, ZPPs, SPs and SPPs) were high, indicating the successful preparation of the particles.

As shown in Fig. 1a & b, ZPs were nearly spherical, while ZPPs agglomerated with each other. This effect was primarily attributed to pectin forming an elastic network gel on the surface of the particles (Fig. 1b). A similar phenomenon was found in the study of Jiang et al[21]. Particles derived from zein/apple pectin tended to clump together and form a lamellar layer in their investigation. Spherical particles were also observed in SPs (Fig. 1c). SPI particles exhibited an irregular structure, which changed to uniformly spherical particles when phytosterol ester was bounded to SPI[14]. These results indicated that there were interaction between stigmasterol and SPI. Stigmasterol crystals exposed to the surface of particles could be observed from the SEM images of SPs (Fig. 1c), which led to the coarser surface of SPs compared to ZSs. It has also been reported in other studies that the surface morphology becomes rougher when certain curcumin crystals appear on the surface of the protein nanoparticles[22,23]. However, no similar phenomenon was observed in the SEM images of SPPs (Fig. 1d), indicating that stigmasterol was completely encapsulated in SPPs. This could be well confirmed by the TEM images of SPs and SPPs in other studies[18]. Protein aggregation may be prevented and particle spatial stability may be increased as a result of the interaction between pectin and SPI.

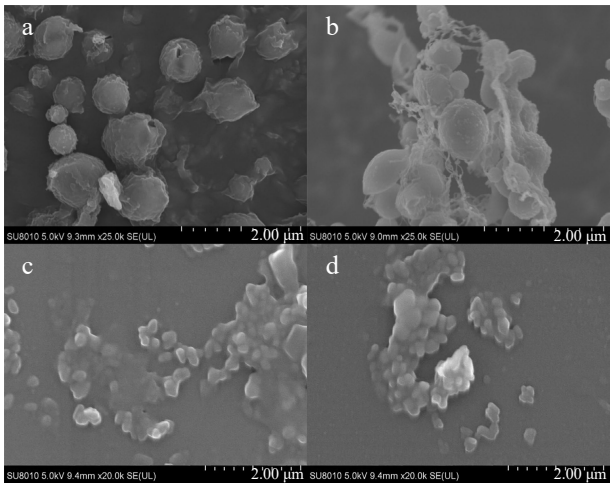

Fig. 1 SEM images of (a) ZPs, (b) ZPPs, (c) SPs and (d) SPPs.

GC–MS ion chromatograms of stigmasterol and POPs

As shown in Fig. 2a, the retention time of stigmasterol was 15.2 min. Figure 2a & b revealed that under the same GC-MS conditions, the peak with a retention time of 15.2 min disappeared, and POPs were well separated in Fig. 2b, indicating that the separation of stigmasterol and POPs by SPE was effective.

Qualitative analysis of POPs was conducted based on the characteristic fragment ions of mass spectrum and the law of mass spectrometry. The derivatives of POPs were analyzed, and the major fragment ions of stigmasterol oxides were referred to a previous study[24]. The peaks in Fig. 2b were analyzed to determine the peak sequence of the main POPs. Among them, 7-ketostigmasterol had the largest polarity and the longest retention time, while 19-hydroxycholesterol had the smallest polarity and the shortest retention time. The remaining POPs were 7α-hydroxystigmasterol, 7β-hydroxystigmasterol, 5β,6β-epoxystigmasterol, and 5α,6α-epoxystigmasterol, arranged in ascending order of polarity.

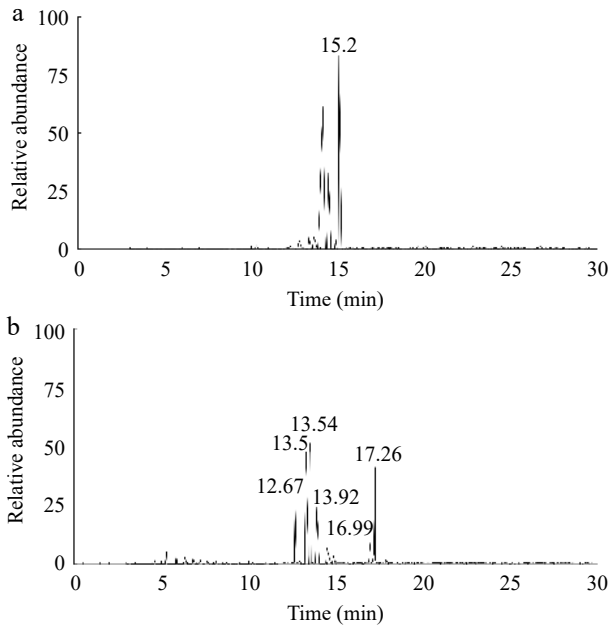

Fig. 2 GC–MS ion chromatograms of (a) stigmasterol and (b) POPs.

Mass spectra of POPs

The molecular ion peaks were observed in POP mass spectra (Fig. 3). The molecular ion peak for both the 7- and 7-hydroxy derivatives was at m/z 572, while their base peaks were both at m/z 482 (M+-90). The 7-hydroxyl derivative showed a distinctive fragment ion peak at m/z 355 (Fig. 3b), whereas the 7-hydroxyl derivative did not, and its distinctive fragment ion peak occurred at m/z 255 (M-side chain-2TMSOH) (Fig. 3a). 7α- and 7β-hydroxyl derivatives were prone to lose the fragment C_1, C_3+TMSO and form the fragment ion of m/z 129[25]. The characteristic fragment ions of both derivatives were m/z 467 (M+-90-15), m/z 392 (M+-180), m/z 343 (M+-90-side chain), and m/z 253 (M+-180-side chain)[26].

The molecular ion peaks of the 5α,6α-epoxide derivative and the 5β,6β-epoxide derivative were observed at m/z 500. Additionally, the relative abundance of the m/z 482 peak of the 5α,6α-epoxide derivative (Fig. 3c) was higher compared to that of the 5β,6β-epoxide derivative (Fig. 3d). Meanwhile, the relative abundance of the m/z 485 peak of the 5β,6β-epoxide derivative was higher than that of the 5α,6α-epoxide derivative. The 5β,6β-epoxide derivative was prone to losing the fragment C_1, C_3+TMSO, and methyl, resulting in the formation of the fragment ion of m/z 129 and m/z 485 (M-CH3), respectively[25]. Other characteristic fragment ions of the 5α,6α-epoxide derivative were m/z 410 (the C-O bond connecting trimethylsilylation was broken, M^+-TMSOH), m/z 377 (M^+-90-18), m/z 271 (M^+-side chain-90), and m/z 382[27].

The molecular ion peak of 7-ketostigmasterol was found at m/z 498 (M^+) as a derivative of trimethylsilyl ethers (Fig. 3e). In the instance of the 7-keto derivative, the side chain was easily broken, leading in the creation of the m/z 359 fragment ion.

When the C-O bond connecting trimethylsilylation was broken, the side chain was lost, and the fragment ion of m/z 269 was formed. The 7-keto derivative was prone to losing the fragment C_1, C_3+TMSO, resulting in the formation of the characteristic fragment ion of m/z 129. It was also easy to lose isopropyl, which led to the production of the distinctive m/z 455 fragment ion. M-(C_8H_{15}+H) at m/z 386 was another distinctive fragment ion of 7-ketostigmasterol[24].

UV oxidation stability of stigmasterol

Figure 4a displays the remaining stigmasterol levels during the entire UV light treatment. As the exposure time increased, the remaining stigmasterol levels gradually decreased. After 60 min of UV irradiation, the remaining stigmasterol decreased from 95.69% to 66.13% in ZPs, from 96.78% to 60.24% in ZPPs, from 96.25% to 46.22% in SPPs, and from 96.27% to 29.38% in

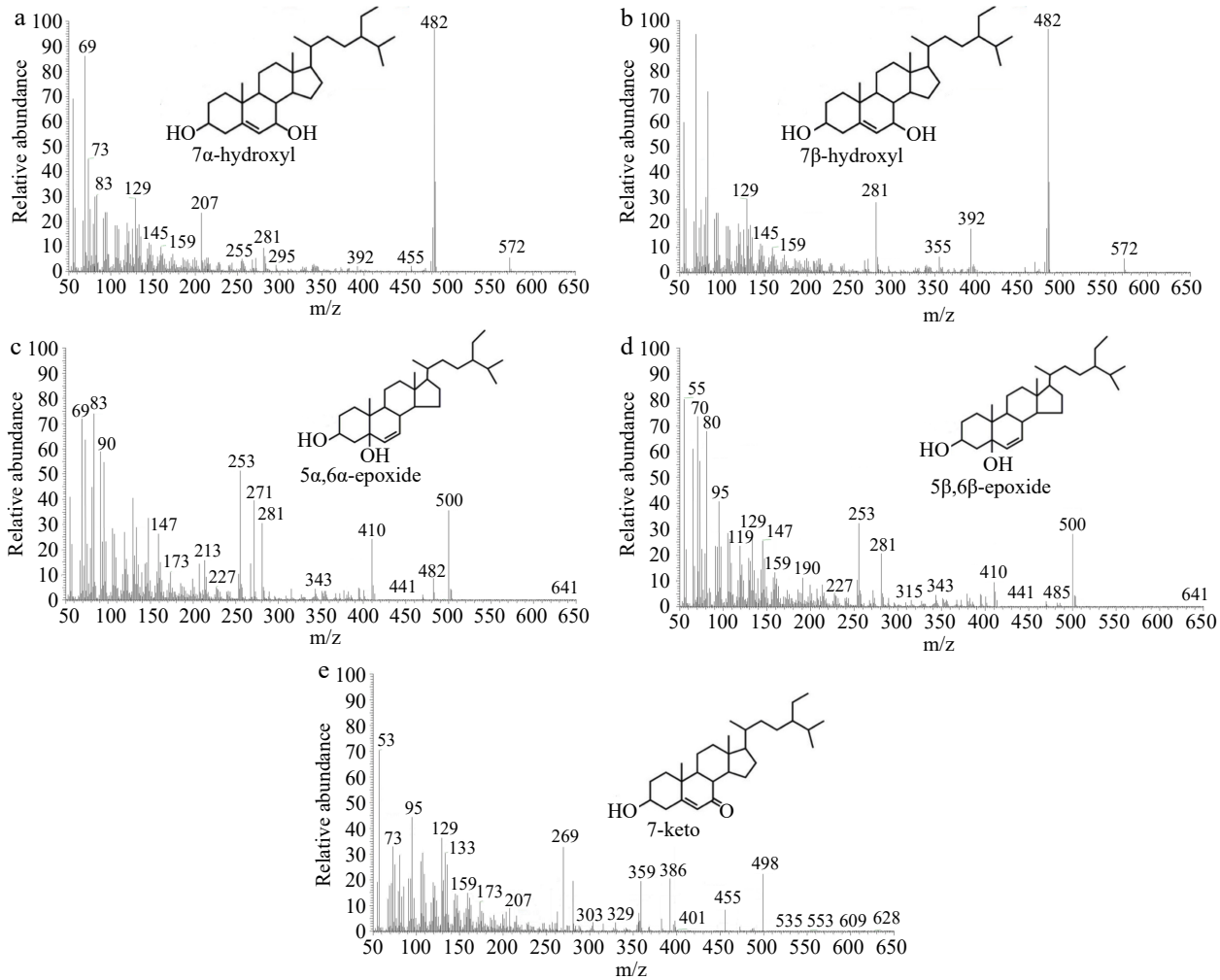

Fig. 3 Mass spectra of (a) 7α -hydroxy, (b) 7β-hydroxy, (c) 5α,6α-epoxy, (d) 5β,6β-epoxy and (e) 7-keto.

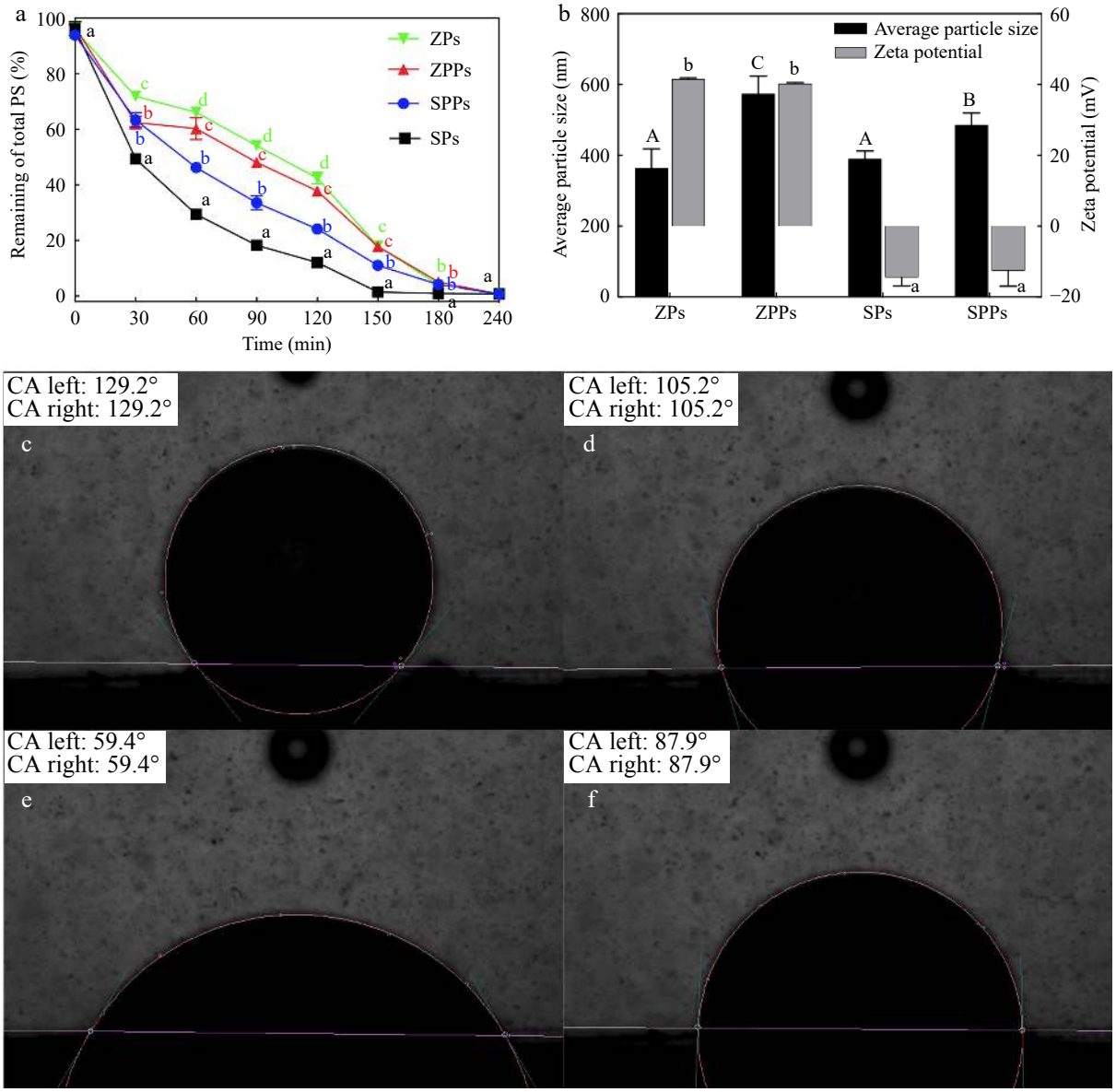

Fig. 4 (a) Remaining percentage of total stigmasterol. (b) Average particle size and zeta-potential of particles. The three-phase contact angle of (c) ZPs, (d) ZPPs, (e) SPs and (f) SPPs.

SPs. There were obvious differences in the amounts of stigmasterol left in each particle at this stage (60 min). The degradation rate order of stigmasterol was SPs > SPPs > ZPPs > ZPs. The presence of pectin significantly improved the UV oxidation stability of stigmasterol in SPPs compared to SPs. In contrast, the UV oxidation stability of stigmasterol in ZPPs significantly decreased compared to ZPs.

In addition, the mean particle size, zeta potential, and hydrophobicity of the particles (ZPs, ZPPs, SPs and SPPs) were investigated. The average particle sizes of ZPs, ZPPs, SPs and SPPs were 364.05 ± 54.30 nm, 574.39 ± 49.55 nm, 390.48 ± 21.53 nm and 486.60 ± 32.99 nm, respectively. The absolute zeta-potential of ZPs and ZPPs was greater than 40 mV, demonstrating the high stability of the particles. The absolute value of zeta-potential of SPs and SPPs was 14.5 ± 2.37 mV and 12.55 ± 4.39 mV, respectively. The results showed that the stability of SPs and SPPs was lower than that of ZPs and ZPPs.

Through hydrophobic contact, stigmasterol was adsorbed onto the surface of SPI particles.[16] and encapsulated in the interior of zein particles during the self-assembly process[15]. Pectin was adsorbed on the particle surface by electrostatic interaction in ZPPs[17] and hydrophobic interaction in SPPs. From a spatial position perspective, the network gel formed by pectin outside the particles could prevent stigmasterol in SPPs from being directly exposed to UV light. However, this blocking effect on stigmasterol in ZPPs was not significant.

The oxidation stability of particles largely depended on the properties of the droplet interface, including specific surface area, composition, and structure[14]. Large emulsion droplets provided a smaller specific surface area for UV degradation, resulting in better protective effects[28]. Therefore, due to their smaller size, SPs were more sensitive to oxidation than SPPs. This result was consistent with the study performed by Zou et al.[28], who proved that colloidal particles of the zein/tannic acid

(ZTPE) complex had better protective effects against curcumin photooxidation than emulsions stabilized with sodium caseinate (SCE). It was because ZTPE had larger droplet size than SCE. Similar to other components such as lipids and pigments, SPI was vulnerable to oxidation during processing and storage[29], which could lead to disulfide bond breaking and reducing the hydrophobicity of the surface[30]. Additionally, some unloaded stigmasterol crystals in SPs were directly exposed to ultraviolet radiation and degraded rapidly[28].

The particle contact angle was measured to investigate the relationship between oxidation stability and particle hydrophobicity. The contact angle was 129° for ZPs (Fig. 4c) and 105° for ZPPs (Fig. 4d). In contrast, we found that the contact angle was around 59° for SPs (Fig. 4e) and around 90° for SPPs (Fig. 4f). The finding revealed a positive correlation between particle hydrophobicity and stigmasterol's photooxidation stability. The presence of zein improved the UV oxidation stability of stigmasterol in ZPs because zein is a hydrophobic protein with oxygen barrier and antioxidant properties[11]. Additionally, the tyrosine and aromatic amino acid residues of zein's conjugated double bonds exhibited the capacity to absorb UV light, which would prevent stigmasterol from degrading[28]. However, oxidation seemed to be further promoted by an increase in hydrophilicity. For ZPPs, electrostatic contact caused pectin to be adsorbed onto the hydrophobic zein surface[17], forming a hydrophilic interface that might promote oxidation.

POPs in the first oxidation stage

To determine the change in oxidation stability of stigmasterol in different particles, POPs were quantitatively analyzed. As shown in Figs 5 & 6, the content of POPs increased over time in the four particles. The order of the generation rate of POPs was SPs > SPPs > ZPPs ≈ ZPs. Compared with ZPs, the oxidation stability of stigmasterol in ZPPs decreased, which was consistent with the results reported previously. The content of the five POPs in ZPPs were higher than those in ZPs (Figs 5 & 6). On the contrary, the contents of the five POPs in SPs were higher than those in SPPs.

When stigmasterol was exposed to reactive oxygen species, it was automatically oxidized at the C-7 position, where the hydrogen atom of the allyl group was abstracted to form a free radical and react with molecular oxygen species ($^3O_2$). When exposed to singlet oxygen ($^1O_2$), which was found to be 1,500 times more reactive than ozone during the photooxidation process, stigmasterol slowly oxidized to 7α-hydroperoxy and 7β-hydroperoxy, then disintegrated to 7α-hydroxy, 7β-hydroxy, and 7-keto[31,32]. The most abundant POPs in SPs was 7β-Hydroxy (Fig. 5a), and its content (8,945 ± 43 μg/g at 240 min) was higher than that of 7α-hydroxy (8,145 ± 62 μg/g at 240 min) (Fig. 5b) and 7-keto (3,015 ± 313 μg/g at 240 min) (Fig. 5c). This was due to the fact that the α-epimer was less popular in terms of thermodynamics[19]. The outcomes demonstrated that the C-7 photooxidation pathway was the most essential pathway in this study[33]. While 7-hydroxy had the highest concentration in this investigation, 7-keto, 7-hydroxy, 7-epoxy, 7-epoxy, and triol were shown to have the highest concentrations of cholesterol oxidation products (COPs)[34]. The difference could be related to the way of oxidation. During heating and pressurization, the epimeric 7-hydroperoxycholesterol was more conducive to dehydrate than the epimeric 7-hydroxycholesterol to form 7-ketocholesterol[34].

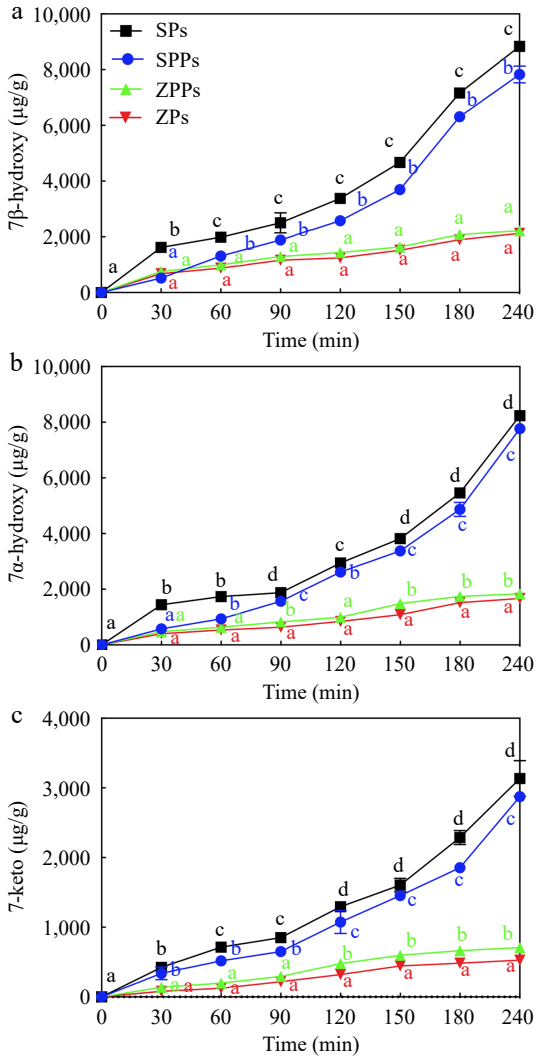

Fig. 5 POPs content derived from (a) 7β-hydroxy, (b) 7α-hydroxy and (c) 7-keto in particles under UV light exposure.

POPs in the second oxidation stage

In the process of epoxidation, stigmasterol oxidized to 5α, 6α-epoxy (Fig. 6a) and 5β, 6β-epoxy (Fig. 6b) by hydroperoxides[35] and their creation was the result of a biomolecular interaction between intact sterols and hydroperoxides. The content of 5,6-epoxy increased significantly after 120 min of UV irradiation (Fig. 6b), which reached 6,010 ± 289 μg/g and 2,822 ± 186 μg/g for 5β,6β-epoxy and 5α,6α-epoxy at 240 min in SPs. These content even exceeded that of 7-keto at the end of photooxidation. The increase in 5,6-epoxy might be due to the increase of free radicals and further photooxidation. The C-5 and C-6 locations of stigmasterol's double bond were damaged by free radicals. After being exposed to LED light for eight days, similar results were observed[19]. During the photooxidation, other breakdown products like dimers, trimers, oligomers, and volatile compounds were also produced. As a result, the amount of POPs produced was always lower than the reduced amount of stigmasterol[36,37].

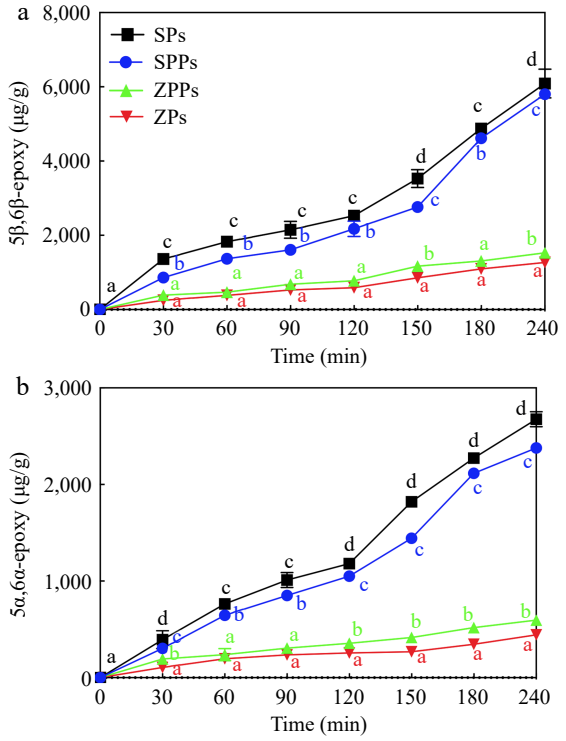

Fig. 6 POPs content derived from (a) 5*α*,6*α*-epoxy and (b) 5*β*,6*β*-epoxy in particles under UV light exposure.

Conclusions

The study examined the effects of different wall materials and spatial positions on the photooxidation stability of stigmasterol. The order of the degradation rate of stigmasterol in different particles was SPs > SPPs > ZPPs ≈ ZPs. The results showed that the relative spatial position of stigmasterol in different particles was the most important factor affecting the photooxidation stability of stigmasterol. Stigmasterol adsorbed on the surface of particles was more easily oxidized by UV light than that encapsulated in the interior of particles. However, this phenomenon could be improved by adding pectin, because the network gel formed by pectin could prevent the direct exposure of stigmasterol to UV light. In addition, the study found that the hydrophobicity of particles was positively correlated with the photooxidation stability of stigmasterol. In the entire UV irradiation process, 7-hydroxyl was the most critical oxidation product, indicating that the photooxidation at the C-7 position was the most significant pathway.

Acknowledgments

This work was supported by Zhejiang Province Natural Science Foundation (LGD22C200001) and the Key Research and Development Program of Zhejiang province (2021C02019 & 2020C02046).

Conflict of interest

The authors declare that they have no conflict of interest.

Dates

Received 25 May 2023; Accepted 24 August 2023; Published online 18 September 2023

References

1. Feng S, Dai Z, Liu A, Wang H, Chen J, et al. 2017. *β*-Sitosterol and stigmasterol ameliorate dextran sulfate sodium-induced colitis in mice fed a high fat Western-style diet. *Food & Function* 8:4179–86
2. Bai G, Ma C, Chen X. 2021. Phytosterols in edible oil: Distribution, analysis and variation during processing. *Grain & Oil Science and Technology* 4:33–44
3. García-Llatas G, Rodríguez-Estrada MT. 2011. Current and new insights on phytosterol oxides in plant sterol-enriched food. *Chemistry and Physics of Lipids* 164:607–24
4. Amir Shaghaghi M, Abumweis SS, Jones PJH. 2013. Cholesterol-lowering efficacy of plant sterols/stanols provided in capsule and tablet formats: Results of a systematic review and meta-analysis. *Journal of the Academy of Nutrition and Dietetics* 113:1494–503
5. Feng S, Dai Z, Liu AB, Huang J, Narsipur N, et al. 2018. Intake of stigmasterol and *β*-sitosterol alters lipid metabolism and alleviates NAFLD in mice fed a high-fat western-style diet. *Biochimica et Biophysica Acta (BBA) - Molecular and Cell Biology of Lipids* 1863:1274–84
6. Hu Y, Ma C, Chen X, Bai G, Guo S. 2022. Hydrophilic phytosterol derivatives: A short review on structural modifications, cholesterol-lowering activity and safety. *Grain & Oil Science and Technology* 5:146–55
7. O'Callaghan Y, McCarthy FO, O'Brien NM. 2014. Recent advances in Phytosterol Oxidation Products. *Biochemical and Biophysical Research Communications* 446:786–91
8. Luister A, Schött HF, Husche C, Schäfers HJ, Böhm M, et al. 2015. Increased plant sterol deposition in vascular tissue characterizes patients with severe aortic stenosis and concomitant coronary artery disease. *Steroids* 99:272–80
9. Feng S, Belwal T, Li L, Limwachiranon J, Liu X, et al. 2020. Phytosterols and their derivatives: Potential health-promoting uses against lipid metabolism and associated diseases, mechanism, and safety issues. *Comprehensive Reviews in Food Science and Food Safety* 19:1243–67
10. Patel AR, Velikov KP. 2014. Zein as a source of functional colloidal nano- and microstructures. *Current Opinion in Colloid & Interface Science* 19:450–58
11. García-Moreno PJ, Mendes AC, Jacobsen C, Chronakis IS. 2018. Biopolymers for the nano-microencapsulation of bioactive ingredients by electrohydrodynamic processing. In *Polymers for Food Applications*, ed. Gutiérrez T. Switzerland: Springer, Cham. pp. 447–79. https://doi.org/0.1007/978-3-319-94625-2_17
12. Wang L, Mu RJ, Li Y, Lin L, Lin Z, et al. 2019. Characterization and antibacterial activity evaluation of curcumin loaded konjac glucomannan and zein nanofibril films. *LWT - Food Science and Technology* 113:108293
13. Zhang L, Liu Z, Wang X, Dong S, Sun Y, Zhao Z. 2019. The properties of chitosan/zein blend film and effect of film on quality of mushroom (*Agaricus bisporus*). *Postharvest Biology and Technology* 155:47–56
14. Chen S, Zhang N, Tang C. 2016. Influence of nanocomplexation with curcumin on emulsifying properties and emulsion oxidative stability of soy protein isolate at pH 3.0 and 7.0. *Food Hydrocolloids* 61:102–12
15. Feng S, Wang Z, Zhao J, Luo Z, Shao P, et al. 2020. Fabrication and characterization of water-soluble phytosterol ester nanodispersion by emulsification-evaporation combined ultrasonic method. *Journal of Food Engineering* 276:109895

16. Feng S, Zheng X, Luan D, Shao P, Sun P. 2019. Preparation and characterization of zein-based phytosterol nanodispersions fabricated by ultrasonic assistant anti-solvent precipitation. *LWT* 107:138−44
17. Feng S, Wang D, Gan L, Shao P, Jiang L, Sun P. 2020. Preparation and characterization of zein/pectin-based phytosterol nanodispersions and kinetic study of phytosterol release during simulated digestion *in vitro*. *LWT - Food Science and Technology* 128:109446
18. Feng S, Yan J, Wang D, Jiang L, Sun P, et al. 2021. Preparation and characterization of soybean protein isolate/pectin-based phytosterol nanodispersions and their stability in simulated digestion. *Food Research International* 143:110237
19. Zhao Y, Yang B, Xu T, Wang M, Lu B. 2019. Photooxidation of phytosterols in oil matrix: Effects of the light, photosensitizers and unsaturation degree of the lipids. *Food Chemistry* 288:162−69
20. Zhou F, Huang X, Wu Z, Yin S, Zhu J, et al. 2018. Fabrication of zein/pectin hybrid particle-stabilized Pickering high internal phase emulsions with robust and ordered interface architecture. *Journal of Agricultural and Food Chemistry* 66:11113−23
21. Jiang Y, Zhang C, Yuan J, Wu Y, Li F, et al. 2019. Effects of pectin polydispersity on zein/pectin composite nanoparticles (ZAPs) as high internal-phase Pickering emulsion stabilizers. *Carbohydrate Polymers* 219:77−86
22. Dai L, Wei Y, Sun C, Mao L, McClements DJ, et al. 2018. Development of protein-polysaccharide-surfactant ternary complex particles as delivery vehicles for curcumin. *Food Hydrocolloids* 85:75−85
23. Liang H, Zhou B, He L, An Y, Lin L, et al. 2015. Fabrication of zein/quaternized chitosan nanoparticles for the encapsulation and protection of curcumin. *RSC Advances* 5:13891−900
24. Dutta PC, Appelqvist LÅ. 1997. Studies on phytosterol oxides. I: Effect of storage on the content in potato chips prepared in different vegetable oils. *Journal of the American Oil Chemists' Society* 74:647−57
25. Johannes C, Lorenz RL. 2004. Preparation and mass spectrometry of 14 pure and $^{18}O_2$-labeled oxidation products from the phytosterols β-sitosterol and stigmasterol. *Analytical Biochemistry* 325:107−16
26. Dutta PC. 1997. Studies on phytosterol oxides. II: Content in some vegetable oils and in French fries prepared in these oils. *Journal of the American Oil Chemists' Society* 74:659−66
27. Soupas L, Juntunen L, Säynäjoki S, Lampi AM, Piironen V. 2004. GC-MS method for characterization and quantification of sitostanol oxidation products. *Journal of the American Oil Chemists' Society* 81:135−41
28. Zou Y, Zhong J, Pan R, Wan Z, Guo J, et al. 2017. Zein/tannic acid complex nanoparticles-stabilised emulsion as a novel delivery system for controlled release of curcumin. *International Journal of Food Science and Technology* 52:1221−28
29. Chen N, Zhao M, Sun W, Ren J, Cui C. 2013. Effect of oxidation on the emulsifying properties of soy protein isolate. *Food Research International* 52:26−32
30. Li J, Wang B, Fan J, Zhong X, Huang G, et al. 2019. Foaming, emulsifying properties and surface hydrophobicity of soy proteins isolate as affected by peracetic acid oxidation. *International Journal of Food Properties* 22:689−703
31. Brzeska M, Szymczyk K, Szterk A. 2016. Current knowledge about oxysterols: A review. *Journal of Food Science* 81:R2299−R2308
32. Bortolomeazzi R, De Zan M, Pizzale L, Conte LS. 1999. Mass spectrometry characterization of the 5α-, 7α-, and 7β-hydroxy derivatives of β-sitosterol, campesterol, stigmasterol, and brassicasterol. *Journal of Agricultural and Food Chemistry* 47:3069−74
33. Scholz B, Guth S, Engel KH, Steinberg P. 2015. Phytosterol oxidation products in enriched foods: Occurrence, exposure, and biological effects. *Molecular Nutrition & Food Research* 59:1339−52
34. Clariana M, García-Regueiro JA. 2011. Effect of high pressure processing on cholesterol oxidation products in vacuum packaged sliced dry-cured ham. *Food and Chemical Toxicology* 49:1468−71
35. Lampi AM, Juntunen L, Toivo J, Piironen V. 2002. Determination of thermo-oxidation products of plant sterols. *Journal of Chromatography B* 777:83−92
36. Derewiaka D, Molińska (née Sosińska) E. 2015. Cholesterol transformations during heat treatment. *Food Chemistry* 171:233−40
37. Menéndez-Carreño M, Ansorena D, Astiasarán I, Piironen V, Lampi AM. 2010. Determination of non-polar and mid-polar monomeric oxidation products of stigmasterol during thermo-oxidation. *Food Chemistry* 122:277−84